Diffraction pattern sampling using a computer-generated hologram

David Casasent, Shao-Feng Xia, Jian-Zhong Song, and Andrew J. Lee

A grating computer-generated hologram (CGH) to perform wedge and ring detector diffraction pattern sampling is discussed. Undesirable effects that result due to the nonparallel light incident on a Fourier transform plane CGH are addressed, and several optical system solutions are suggested. Experimental demonstrations are provided.

I. Introduction

Traditional optical processors are linear space-invariant systems. Their basic operation is based on the Fourier transform (FT) property of a lens.[1] Recently, much interest exists in nonlinear and space-variant systems because of the limited applications of linear space-invariant systems. One suggested space-variant system combines a space-invariant system with a coordinate transformation (CT) for distortion-invariant correlation and pattern recognition.[2] Implementation of the coordinate transformation by computer-generated holograms (CGHs) is particularly attractive.[3–7] The use of holographic optical element[8] and CGH[9] techniques to achieve diffraction pattern sampling with unusually shaped detectors (usually wedge and ring shaped detector elements) is another application that has received recent attention.

In Sec. II, we discuss the concept of a wedge ring detector (WRD) CGH for diffraction pattern sampling. The CGH techniques for such applications are based on the principle of grating diffraction in local regions of the CGH. In such cases, light incident on the CGH must be parallel to the optical axis. When the CGH is used for diffraction pattern sampling, or when the CGH must compute the CT of FT plane data (as is needed to achieve shift-invariance), the light incident on the CGH will not be parallel. In Sec. III, we discuss the magnitude of this effect. In Sec. IV, we discuss optical systems that remove problems of nonparallel input light on CGHs. Initial WRD CGH experimental results and initial tests of our optical system to allow the use of such CGHs in an FT plane are presented in Sec. V. The discussion, summary, and conclusion follow in Sec. VI.

II. Computer-Generated Hologram Wedge Ring Detector

The FT of 2-D input data can be easily produced optically and contains much useful information for object identification, orientation, inspection, and metrology. An FT feature space is also well known to allow significant data compression in many cases. Spatial frequency and object scale information is present in the radial distance of FT peaks from the origin, and object orientation information is present in the angular location of FT peaks. A most attractive method of FT plane sampling that allows data compression and retains the above information properties of the FT plane is to use wedge and ring shaped detector elements.[10] Such a wedge and ring sampled FT plane feature space has attractive shift, scale, and rotation invariant properties for pattern recognition.[11] Commercial WRD devices exist and have been demonstrated for many diverse uses.[12]

The WRDs that have thus far been used were fabricated from silicon. However, they are slow (due to the capacitance associated with the large detector areas), have less sensitivity and dynamic range than one can achieve with conventional detectors, and are often expensive. To improve the speed, sensitivity, and dynamic range of such a system and to allow the use of other FT plane sampling geometries, we suggest the use of CGHs for diffraction pattern sampling (Fig. 1). The required CGH (placed in the FT plane P_2) contains wedge and ring shaped regions (with N_W wedge regions in the upper half of the FT plane and N_R ring regions in the lower half of the FT plane). In the realization we consider, each of the $N = N_W + N_R$ regions contains a grating at a given spatial frequency

Shao-Feng Xia is with Fudan University, China; Jian-Zhong Song is with Changchun Institute of Optics & Fine Mechanics, China; the other authors are with Carnegie-Mellon University, Department of Electrical & Computer Engineering, Pittsburgh, Pennsylvania 15213.

Received 20 July 1985.
0003-6935/86/060983-07$02.00/0.

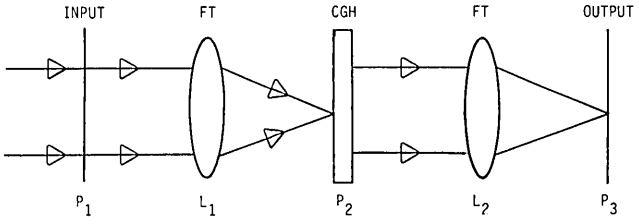

Fig. 1. Basic optical system with a CGH to produce WRD FT plane samping.

and orientation. By varying the spatial frequency and orientation of each grating, the FT plane light amplitude in each of these N regions of P_2 can be collected and redirected by the CGH into N plane waves each leaving P_2 in a different angular direction. A lens L_2 placed behind the CGH (or included on the CGH as a holographic optical element) will collect each of these N plane waves onto separate detectors in spatially different regions in the final output plane P_3. The output from the P_3 detectors now corresponds to the wedge and ring sampled FT plane data.

This grating CGH thus performs a specific type of CT on the FT data at P_2 by redirecting the angular pattern of the light incident on P_2. A binary grating pattern in each CGH region is assumed, since this allows easy replication of the CGH. Only the first order from each such binary grating pattern is used, and the lens and detector system are arranged so that higher diffracted orders do not cause problems. The basic concept can also be used to realize image plane CTs for distortion-invariant pattern recognition. Our present emphasis will be on the case of wedge and ring sampled FT data. The resultant system of Fig. 1 can be quite small (since the size of the CGH can be adjusted to match the FT plane size). This adjustment is much easier with the CGH than with a silicon WRD (where an entirely new detector assembly must be fabricated for different sized FT patterns). With separate detectors of smaller size in P_3, their speed, response, and dynamic range will be much better than for the larger area detectors required at P_2 directly. The system is also attractive because it is not restricted to wedge and ring shaped sampling. (Such sampling is discussed as the most obvious initial example.)

III. Effects of Nonparallel Incident Light on a CGH

Most CGHs that have been demonstrated in the literature were constructed using either the detour phase or binary grating methods.[13] Using the detour phase method, a CGH is made up of small individual cells with an aperture (whose size and position vary) within each cell. In the binary grating method, each CGH region consists of a grating with different frequency and orientation. We now consider the effects of nonparallel incident light on binary grating CGHs, although our analysis may also be extended to detour phase and other CGH coding methods. Our concern is the fact that in many applications of CGHs, the incident light is not parallel. Our present purpose is to quantify this effect (for the case of a WRD FT plane CGH).

We consider a 1-D grating with grating spacing d and input illumination λ. The diffraction angle ϕ for first-order light leaving the grating and the illumination angle θ for input reading light satisfy[14]

$$d(\sin\theta + \sin\phi) = \lambda. \tag{1}$$

Equation (1) clearly shows the dependence of the diffracted light on the incident angle θ. For our case, the light incident on each of the N wedge and ring shaped CGH regions at P_2 will include light with incident angles continuously varying from θ_1 to θ_2. The range of angles θ_1 to θ_2 varies between wedge elements and within ring elements and depends on the input spatial frequencies and where they occur in the input plane P_1 pattern.

For the case of one grating region with incident light in a cone defined by θ_1 and θ_2, the light leaving this CGH region will have a continuous range of angles from ϕ_1 to ϕ_2 (corresponding to θ_1 and θ_2) satisfying Eq. (1). In practice, θ_2 and ϕ_2 will be negative. Our equations assume all angles are positive. The light at the two extreme exiting angles ϕ_1 and ϕ_2 will be focused by L_2 of focal length f_L at y_1 and y_2 in P_3, where

$$y_1 = f_L \tan\phi_2, \qquad y_2 = f_L \tan\phi_1. \tag{2a}$$

The P_3 light from one local CGH grating region thus has a spatial extent in y of

$$A = y_1 - y_2 \tag{2b}$$

and is centered at

$$y_c = (A/2) + y_2. \tag{2c}$$

In practical cases, $f_L \gg A$ or $f_L \gg y_1$ and y_2. Thus ϕ_1 and ϕ_2 are small, and $\sin\phi \approx \tan\phi$, and

$$A = f_L(\sin\theta_1 - \sin\theta_2), \tag{3a}$$

$$y_c = (\lambda f_L/d) - (f_L/2)(\sin\theta_1 + \sin\theta_2). \tag{3b}$$

Table I quantifies the size A and location y_c in P_3 to which one local grating region of the CGH at P_2 will focus for several ranges of the incident light angles θ_1 and θ_2 (for the case $f_L = 200$ mm, $\lambda = 0.514$ μm, and $d = 0.05$ mm). From Table I, we note that if $\theta_1 = -\theta_2$, y_c is unchanged, whereas if $\theta_1 \neq \theta_2$, y_c shifts as expected.[1] When $\theta_1 = -\theta_2$, the size of the P_3 output spot increases with θ. For a coordinate transform or WRD CGH, each CGH region will have a different grating orientation (and in general a different grating spatial frequency).[5,8,9] If the P_1 input pattern shifts, the incidence

Table I. Example Calculation Results

Incident angles θ_1(deg)	Incident angles θ_2(deg)	Size A (mm)	Position y_c (mm)
0.2	−0.2	1.4	2.1
0.5	−0.5	3.5	2.1
1.0	−1.0	7.0	2.1
0.2	−0.8	3.5	3.1
0.8	−0.2	3.5	1.1

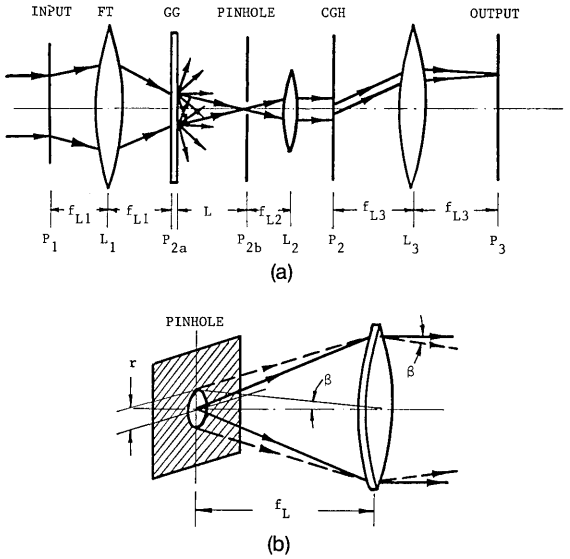

Fig. 2. Preferred optical system for CGH wedge and ring FT plane sampling: (a) quasi-parallel light system; (b) details of the pinhole and lens L_2 system.

angles θ vary and so do the P_3 output locations and size (for each CGH grating). This can easily cause P_3 data to overlap. Thus the P_3 output will not be shift-invariant. From Table I, the size and location of the P_3 output for one CGH grating are seen to vary significantly with realistic ranges of θ. This variation is such that P_3 outputs from separate CGH gratings will overlap, even without shifts of the P_1 input. For these reasons, methods to overcome the θ variations are needed for grating CGHs used in an FT plane. Section IV addresses solutions to this issue.

IV. Quasi-parallel System for Eliminating the Effects of Nonparallel Incident Light

The system of Fig. 2(a) is one solution to the CGH problems mentioned above. This system includes ground glass (GG) at the FT plane P_{2a} (to produce spatially incoherent light) and a pinhole a distance L from the GG. (This forms a pinhole camera that images P_{2a} onto the plane of L_2.) We refer to light leaving the lens L_2 as quasi-parallel because the pinhole is a point source of finite size at the front focal plane of L_2. The CGH is now placed behind L_2 at P_2, and the output FT lens L_3 forms the WRD sampled FT pattern on discrete detectors in P_3.

If we denote the input image at P_1 by $f(x,y)$ and its FT incident at P_{2a} by

$$F(u,v) = [F(u,v)|\ \exp[j\Phi(u,v)] \tag{4}$$

the purpose of the ground glass and pinhole system is to remove the $\Phi(u,v)$ term that describes the direction of the input P_{2a} light, since this is the cause for the CGH problems noted in Sec. III. Because of the finite pinhole size, the light incident on P_2 will only be approximately parallel with a divergence angle β [see Fig. 2(b)]. The diameter of the pinhole must be chosen small enough so that it will image but not so small that diffraction effects become apparent. According to Lord Rayleigh,[15] the optimum pinhole radius r that will give the best resolution satisfies

$$r^2[(L + f_L)/Lf_L] = 0.9\lambda, \tag{5}$$

where L is much greater than the spatial extent of the plane being imaged. If $L = f_L$, solving Eq. (5) for r yields

$$r = 0.67(\lambda f_L)^{1/2}. \tag{6}$$

The divergence angle β [see Fig. 2(b)] is also the angle subtended by the pinhole. Suppose that $\lambda = 0.514\ \mu$m and $L = f_L = 200$ mm, using Eq. (6) we obtain $r = 0.21$ mm. Clearly, $r \ll f_L$. For this case

$$\beta \approx r/f_L = 0.67(\lambda/f_L)^{1/2}. \tag{7}$$

Using our values above, $\beta = 0.001$ rad, and nearly perfect parallel output light results.

The method in Fig. 2 was detailed because it was the one used in our laboratory demonstrations (Sec. V). The system of Fig. 2 is a modified version of an earlier system[16] for speckle removal in coherent readout imaging. It suffers from a large loss in usable light. An alternate method (Fig. 3) involves placing a 2-D spatial light modulator (SLM) such as a liquid crystal light valve (LCLV)[17] in the FT plane. In this case, the FT data are written on the left side of the LCLV in λ_2 light, and the recorded pattern is read out in parallel in λ_1 light in reflection. The system of Fig. 3 is more complex (two wavelengths of light are required) and more expensive (because of the extra LCLV SLM required). Preferable methods would employ other types of CGH or would include spatial correction for the θ variations in each CGH region. This would require nonuniform gratings in each region of the FT plane and increase CGH recording requirements. Such effects can be quantified for specific applications and FT systems.

V. Experimental Results

Several CGH experiments were performed on the systems of Figs. 1 and 2(a). The CGH used in our experiments consisted of wedge and ring shaped grating elements to model a WRD diffraction pattern sampler. The gratings were arranged to focus wedge and ring outputs to spots in two annular regions in P_3 [see

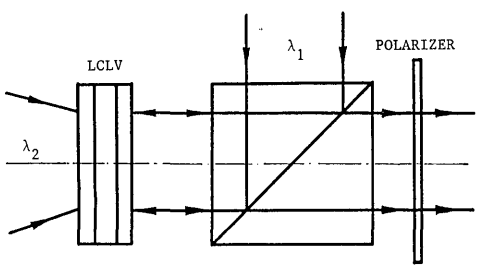

Fig. 3. Use of a liquid crystal light valve to form parallel light.

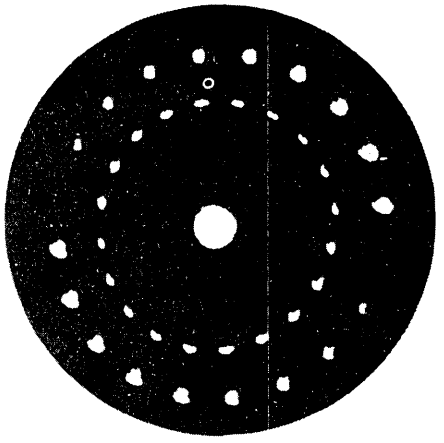

(a)

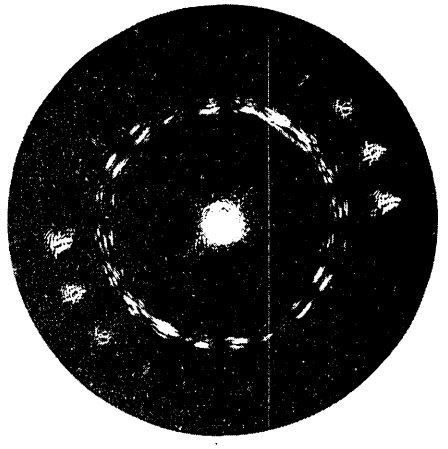

(b)

Fig. 4. Diffraction pattern of a WRD CGH with (a) parallel incident light and (b) nonparallel convergent incident light.

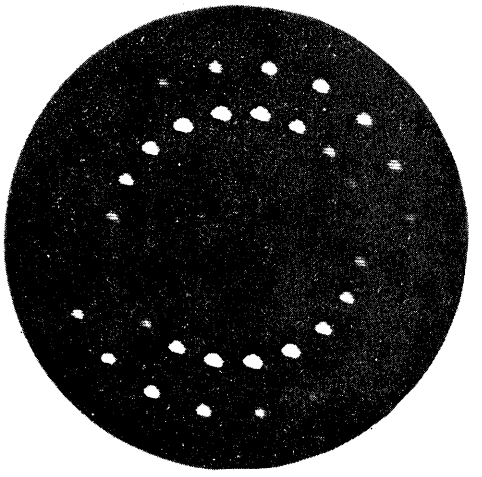

(a)

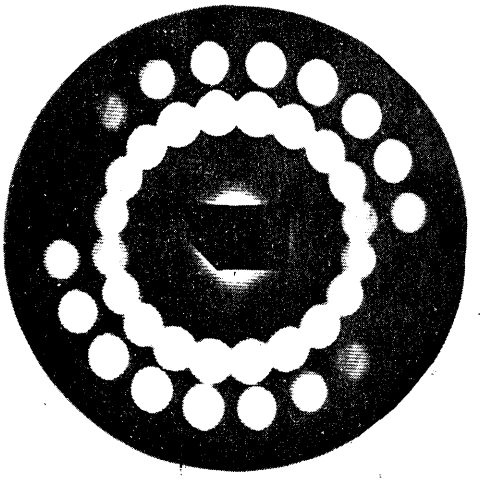

(b)

Fig. 5. Diffraction pattern at P_3 of Fig. 2(a) with a circular input aperture and with different size pinholes of radius (a) $r = 0.25$ mm and (b) $r = 0.85$ mm.

Fig. 4(a)]. Gratings to produce wedge and ring outputs in a rectangular pattern in P_3 are also possible. The system used $\lambda = 0.5145$ μm, an incident light power of 0.5 W, $f_L = 381$ mm, and $L = 192$ mm. When the WRD CGH in Fig. 1 was uniformly illuminated with parallel light, the pattern in Fig. 4(a) results. When illuminated with nonparallel convergent light with converging cone angle $\theta \approx 0.86°$, the pattern in Fig. 4(b) resulted. The outer ring of peaks corresponds to the +1- and −1-order diffraction patterns from the ring shaped CGH elements. The inner circle corresponds to the outputs for the wedge shaped CGH elements. Ten wedge and ten ring CGHs were used for all tests. The spots in Fig. 4(a) are much more well defined and focused, as expected. In all output figures, the different sizes of each CGH region and the different modulation in each CGH region (due to MTF effects) result in intensity variations in the output patterns for the different CGH regions. Such effects will not exist in practice with gain adjustments included on the P_3 detectors.

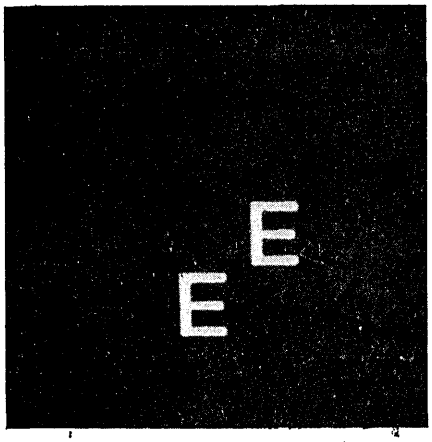

Fig. 6. Input image used in our experiments.

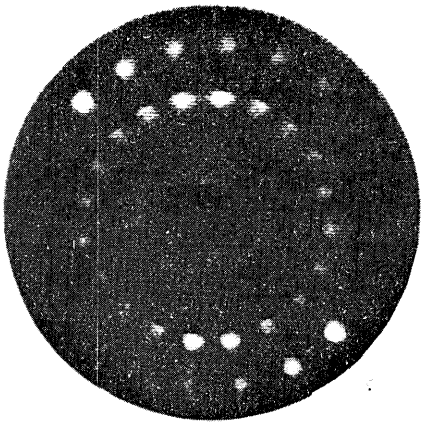

(a)

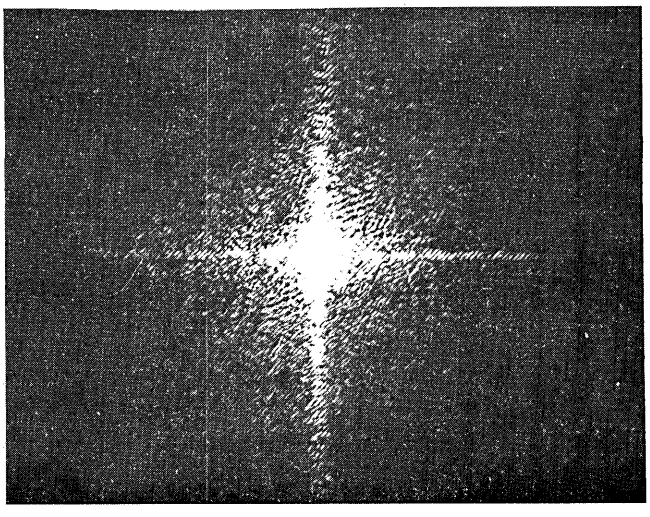

(b)

Fig. 7. (a) Resulting diffraction pattern in Fig. 2(a) with the letters E as input; (b) FT spectrum of light.

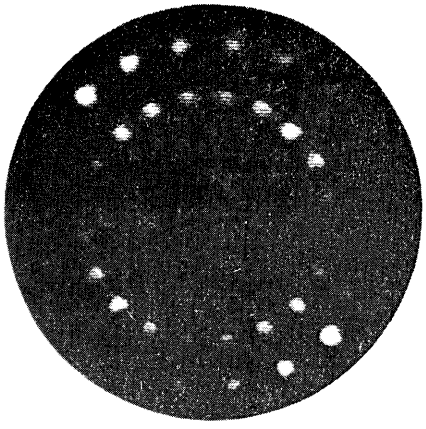

(a)

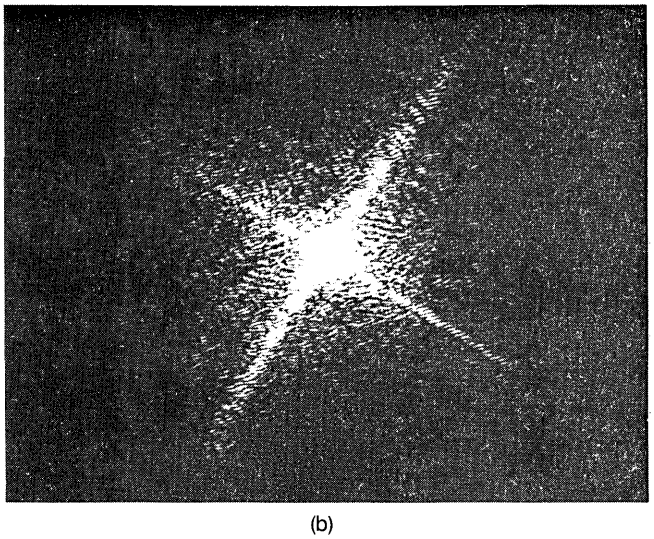

(b)

Fig. 8. Same as Fig. 7 but with the input rotated clockwise by 35°.

When the system of Fig. 2(a) was used with a circular input object of 5-mm diameter at P_1, the P_3 output patterns in Fig. 5 resulted with different pinholes used at P_{2b} of Fig. 2(a). From Eq. (5), we calculate the optimum pinhole size $r = 0.24$ mm. In Fig. 5(a), the size of the pinhole used was $r = 0.25$ mm (the closest size available), and in Fig. 5(b) it was increased to $r = 0.85$ mm. The diffraction pattern samples in Fig. 5(a) are better defined than those in Fig. 5(b), as expected. Without the pinhole, only a large output blob resulted. When pinholes smaller than $r = 0.25$ mm were used, diffraction effects arose, and the diffraction pattern in the output was very faint.

To verify that the WRD CGH used in the system of Fig. 2(a) forms the proper FT pattern, other experiments were performed using the two translated images of the letter E (see Fig. 6) as the input pattern at P_1 in Fig. 2(a). Figure 7(b) shows the FT light pattern incident on the CGH, and Fig. 7(a) shows the WRD diffraction pattern obtained from the CGH in our quasi-parallel light system. Figures 8(a) and (b) and 9(a) and (b) show the same results when the input image in Fig. 6 was rotated clockwise and counterclockwise by 35°. As before, from Figs. 7(a), 8(a), and 9(a) we see that the ring outputs do not change when the input image was rotated and that the peak positions of the wedge outputs translate around the inner ring as the input image rotates. This is expected. This verifies the good spot shape provided by our system and its expected performance under input object rotations.

To verify the shift invariance of our processor, the system of Fig. 2(a) was used with the letter E as the input image. One of the diffraction spots in the CGH output plane P_3 was scanned with a photometric microscope. The input image was then shifted by 10 mm, and the same location in P_3 was scanned once again. The two plots are nearly identical, as shown in Fig. 10. The small differences are due to the varying granularity in different spatial regions of the ground glass and its coherent speckle. This verifies that our quasi-

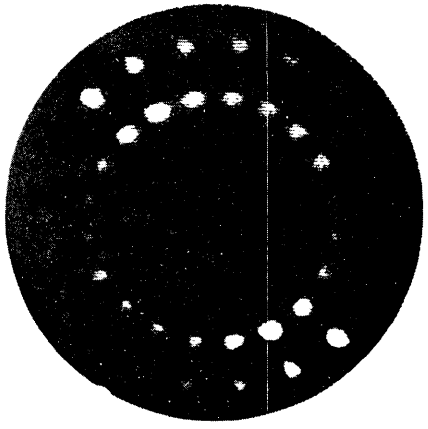

(a)

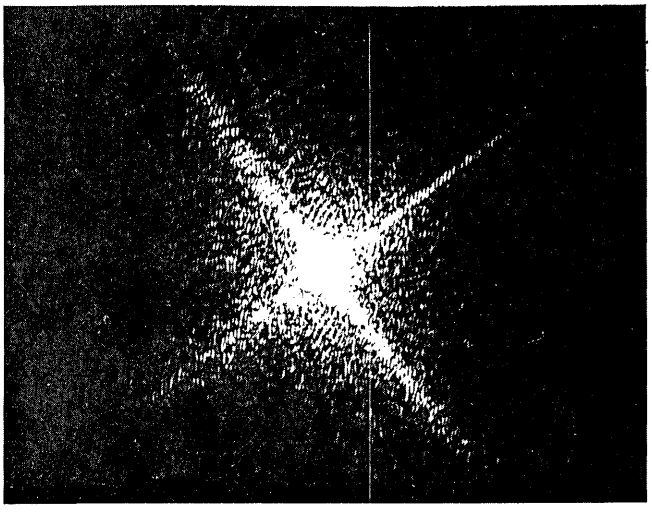

(b)

Fig. 9. Same as Fig. 7 but with the input rotated counterclockwise by 35°.

parallel system is shift invariant and hence removes all incident light angle effects (i.e., input image shifts). Together with the rotation performance noted above, these two results indicate that the WRD CGH performs correctly in the system of Fig. 2(a).

The experiments that we have performed were implemented with rotating ground glass. It is not necessary that the GG be rotated if a GG of very fine granularity is used. When the GG in our experiments was not rotated, the results were similar, except that the intensity of the output spots changed when the input was rotated or shifted. This is due to the different transmittances of the various points on the GG. When the GG is rotated, these points are averaged together, and no amplitude effects are noticed.

VI. Summary and Conclusions

The use of grating computer-generated holograms in optical data processing is considered with emphasis on a CGH to achieve wedge and ring sampled FT plane

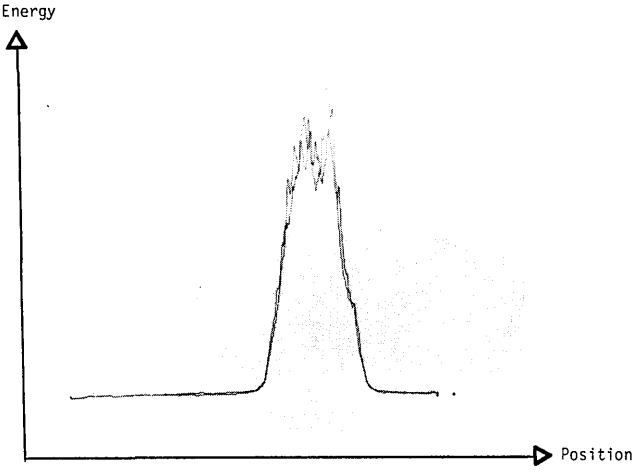

Fig. 10. Two intensity distributions of a diffraction sample with the input unshifted and shifted.

outputs. These outputs are equivalent to those obtained with a FT plane detector with wedge and ring shaped detector elements. The proposed CGH system has size, weight, power dissipation, sensitivity, dynamic range, and speed advantages. The design of this CGH and the effects of nonparallel incident light were provided. Solutions to the nonparallel input light issues were advanced. Laboratory data on the system, its shift-invariance, and rotation-invariance were provided.

The support of this research by an Air Force Office of Scientific Research grant (AFOSR-84-0293) and a DARPA contract is gratefully acknowledged.

References

1. J. W. Goodman, *Introduction to Fourier Optics* (McGraw-Hill, New York, 1968).
2. D. Casasent and D. Psaltis, "Deformation-Invariant, Space-Variant Optical Pattern Recognition," in *Progress in Optics*, E. Wolf, Ed. (North-Holland, New York, 1978), pp. 289–356.
3. O. Bryngdahl, "Geometrical Transformations in Optics," J. Opt. Soc. Am., **64**, 1092 (1974).
4. J. Cederquist and A. Tai, "Computer Generated Holograms for Geometric Transformations," Appl. Opt. **23**, 3099 (1984).
5. H. Bartelt and S. Case, "Coordinate Transformations Via Multifacet Holographic Optical Elements," Opt. Eng. **22**, 497 (1983).
6. D. Casasent and C. Szczutkowski, "Optical Mellin Transforms using Computer Generated Holograms," Opt. Commun. **19**, 217 (1976).
7. Y. Saito, S. Komatsu, and H. Ohzu, "Scale and Rotation Invariant Real Time Optical Correlator Using Computer Generated Hologram," Opt. Commun. **47**, 8 (1983).
8. M. S. Brown,. "A Multifacet Holographic Field Lens for Diffraction Pattern Sampling," Opt. Acta **31**, 507 (1984).
9. D. Casasent and J. Song, "A Computer Generated Hologram for Diffraction Pattern Sampling," Proc. Soc. Photo-Opt. Instrum. Eng. **523**, January (1985).
10. G. G. Lendaris and G. L. Stanley, "Diffraction-Pattern Sampling for Automatic Pattern Recognition," Proc. IEEE **58**, 198 (1979).

11. D. Casasent and V. Sharma, "Feature Extractors for Distortion-Invariant Robot Vision," Opt. Eng. **23**, 492 (1984).
12. H. Kasden and D. Mead, "Out of the Laboratory and into the Factory—Optical Computing Comes of Age," Proc. Elect. Opt. Syst. Des., **248**, 248 (1976).
13. W. H. Lee, "Computer Generated Holograms: Techniques and Applications," in *Progress in Optics*, E. Wolf, Ed. (North-Holland, New York, 1978), pp. 119–232.
14. R. J. Collier, C. B. Burckhart, and L. H. Lin, *Optical Holography* (Academic, New York, 1971).
15. R. W. Wood, *Physical Optics* (Macmillan, New York, 1956).
16. A. Gara, "Optical Computing for Image Processing," in *Computer Vision and Sensor-Based Robots*, G. G. Dodd and L. Rossol, Eds., (Plenum, New York, 1979), pp. 207–237.
17. W. P. Bleha *et al.*, "Application of the Liquid Crystal Light Valve to Real-Time Optical Data Processing," Opt. Eng. **17**, 371 (1978).

Patter *continued from page 961*

Millimeter-wave radiation is generated by the klystron, then chopped by a ferrite modulator at the frequency best suited to the detector used to monitor the sidebands. The chopper output then passes into the waveguide and to the mixer. The laser and klystron signals are mixed nonlinearly in the diode, producing sidebands at the sum and difference frequencies. The unused laser power and the sideband power return to the interferometer along the path of the incident laser beam. The interferometer path difference is chosen so that the sideband polarization is rotated by 90°, and the laser beam is not rotated.

In an ideal Michelson interferometer, all the sideband power and none of the laser power would be reflected out. Because of imperfections in the polarizers and their positioning, some laser power leaks through with the sidebands. A tunable Fabry-Perot interferometer filters most of the laser power out of the beam and selects the desired sideband. Further suppression of the laser component is obtained with a mesh filter that acts as a sharp notch (narrow-band-rejection) filter. The notch frequency is tuned by adjustment of the angle of the filter with respect to the beam.

An absorption cell for spectroscopic studies is placed in the output path. The cell is filled with a material having a spectral absorption line within the frequency range of the mixer output. As the klystron is scanned in frequency, the detector output is recorded to obtain an absorption spectrum of the material.

The system has been demonstrated at several frequency bands. Initially, the laser was operated at the 693-GHz line of formic acid while the klystron was tuned to 93 GHz and chopped at 1 kHz. Linear sweeps of the Fabry-Perot interferometer clearly indicated the generation of both sidebands with an excellent signal-to-noise ratio. Sidebands were also generated at the numerous frequencies up to 3200 GHz. Absorption-cell tests were also successful; for example, by use of the lower sideband of the formic acid line, the klystron was swept in frequency to scan the 599.92681-GHz absorption line of heavy water (HDO).

This work was done by HerbertM. Pickett and Jam Farhoomand of Caltech for NASA's Jet Propulsion Laboratory. Inquiries concerning rights for the commercial use of this invention should be addressed to the Patent Counsel, NASA Resident Office-JPL. Refer to NPO-16497.

Tracking system for IR spectrometer

A visible laser tracking system for an infrared laser spectrometer keeps the probe infrared laser beam aimed at a moving reflector, thereby keeping the reflector image and the return laser beam within the spectrometer field of view. The system includes a tracking mirror that is tilted by stepping motors under microprocessor control to deflect the beams toward the continually changing reflector position.

The tracking system is part of a balloon-borne infrared laser spectrometer that measures the composition of the upper atmosphere at altitudes of ~25–40 km. To reduce the effects of outgassing from the balloon and gondola, the spectrometer measures infrared absorption over a path to and from a reflector hanging as much as 500 m below the gondola. Most of this 1000-m path is far enough away that the effects of outgassing from objects adjacent to the instrument are negligible.

The suspended reflector swings like a pendulum below the instrument gondola. The tracking system, mounted in the gondola, uses a visible light beam from a He–Ne laser, distinct from the spectrometer beam from an infrared laser. The beam is directed to the reflector by mirrors and lenses (see Fig. 17) and broadens to a spot of 2-m diameter at a distance of 500 m. The reflector diameter is 14 cm. The axis of the spectrometer beam is maintained in a fixed orientation relative to that of the tracking beam. The tracking beam returned by the reflector to the gondola is projected on an array of light sensors in a TV camera, and the camera output is fed to the microprocessor and controller.

In the first tracking stage the controller, under direction of the microprocessor, moves the tracking mirror so that the visible laser beam traces a spiral pattern at the reflector distance. As soon as the spiral scan picks up a glint from the reflected, visible tracking beam, the microprocessor moves the tracking mirror to position the glint at the center of a 32-by-32-picture central section of the 64,000-element camera array.

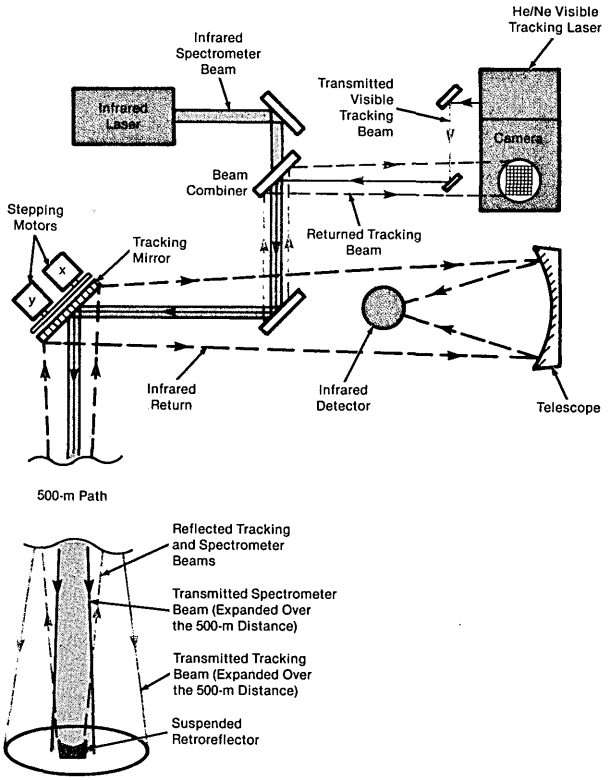

Fig. 17. Motor-driven tracking mirror directs the visible tracking beam and the infrared spectrometer beam toward the reflector. Under microprocessor control, the tracking mirror keeps the beams aimed at the retroreflector.

Every 0.05 s, the microprocessor updates the position of the glint with respect to the center of the array and computes a new scanning velocity that will move the tracking mirror in synchronism with any motion of the reflector. When tracking is fully maintained, the microprocessor turns to a fine-search algorithm, which moves the tracking mirror so that it samples different parts of the reflected tracking beam. At the same time, the microprocessor monitors the infrared beam reflected to the spectrometer receiving telescope. When the returned infrared power reaches a maximum, the system locks on the corresponding visible position for tracking. The fine-search algorithm allows for offset—either intentional or accidental—between the axes of the tracking beam and the spectrometer beam.

This work was done by Robert A. Johnson, Christopher R. Webster, Robert T. Menzies, Guy B. Morrison, and James H. Riccio of Caltech for NASA's Jet Propulsion Laboratory. Refer to NPO-16440.

continued on page 1015